Computational study of Cs immobilization in the apatites $Ca_{10}(PO_4)_6F_2$, $Ca_4La_6(SiO_4)_6F_2$ and $Ca_2La_8(SiO_4)_6O_2$

Alain Chartier and Constantin Meis
Commissariatà l'Energie Atomique, Laboratoire de Chimie Physique et d'Intégration bât. 450, 91191 Gif-Sur-Yvette, France

Julian D. Gale
Department of Chemistry, Imperial College of Science, Technology and Medicine, South Kensington SW7 2AY, United Kingdom
(Received 15 February 2001; published 7 August 2001)

Incorporation and lattice migration of cesium in three apatites fluorapatite $Ca_{10}(PO_4)_6F_2$, lanthanum-fluorobritholite $Ca_4La_6(SiO_4)_6F_2$ and lanthanum-oxyapatite $Ca_2La_8(SiO_4)_6O_2$ have been studied theoretically. The above apatites have been first optimized by applying the *ab initio* Hartree-Fock method using electron core pseudopotentials. Mulliken analysis has shown the calculated anion charges in the apatite tunnels to have formal values, thus establishing the presence of ionic bonds with cations at site II ($6h$), particularly in $Ca_2La_8(SiO_4)_6O_2$. These results have been used for optimizing the corresponding interactions in the interatomic potential method employed in the following. Free energy calculations have shown the preferential site for Cs and La incorporation in the three apatites to be site I (4f) and site II ($6h$), respectively. The calculated activation energies for Cs migration offer evidence that cesium diffusion is mainly controlled by intersite (I↔II) jumps to adjacent vacancies. $Ca_2La_8(SiO_4)_6O_2$ proves to have the higher immobilization capacity, because of the high activation energies characterizing all the possible lattice diffusion mechanisms.

DOI: 10.1103/PhysRevB.64.085110 PACS number(s): 66.30.Jt, 31.15.Qg, 31.15.Ar

I. INTRODUCTION

Apatites found in the Oklo natural reactor have retained an important variety of radionuclides, as well as significant quantities of fission products, in their structures over a geological time period.[1] Hence, in the context of nuclear waste disposal, apatites of the general composition $(Ca,RE)_{10}(SiO_4,PO_4)_6(F,O)_2$ where RE=rare earth elements, have been proposed for actinide immobilization.[2–4] Recent experimental[5] and theoretical studies[6] have envisaged cesium incorporation and immobilization in apatites. Since Cs radionuclides imply no α-recoil damage in the host matrix, the aim of this study is to investigate the Cs immobilization capacity, from the point of view of diffusion, of three representative apatites, namely, fluoroapatite $Ca_{10}(PO_4)_6F_2$, lanthanum-fluorobritholite $Ca_4La_6(SiO_4)_6F_2$ and lanthanum-oxyapatite $Ca_2La_8(SiO_4)_6O_2$. We use two theoretical methods in order to carry out this study: the *ab initio* periodic Hartree-Fock method implemented in the CRYSTAL98 code[7] and interatomic potential modeling as implemented in the GULP program.[8] The coupling of *ab initio* and interatomic potential methods for the study of various crystal lattices has already been applied with success (Stefanovich *et al.*[9] and Tsuneyuki *et al.*[10]). Here, the principal goal of the *ab initio* study is to give insight into the partial electrostatic charges located on the atoms as well as on the nature of the chemical bonds established between them in the apatite structure. Based on these results, the interatomic potential modeling is further optimized in order to obtain an improved description of the apatite crystallographic properties. The established force field is used for the investigation of the site preference of cesium and lanthanum in the apatite structures considered, as well as for the calculation of the activation energies corresponding to various lattice migration mechanisms for the Cs ion.

II. COMPUTATIONAL DETAILS

The implementation of the *ab initio* self-consistent field (SCF) Hartree-Fock Linear Combination of Atomic Orbitals (LCAO) computational scheme within the CRYSTAL98 code[7] has been described in other papers (see, for example, Dovesi *et al.*[11]). Concerning the basis sets, we have used the effective core pseudopotential (ECP) calculated by Hay and Wadt with Gaussian-type orbitals having a contraction of 211G*, for the valence part of calcium ([HAYWSC]-211G*, see Ref. 12), and the ECP obtained by Durand and Barthelat with a valence part of 21G* for silicon ([DURAND]-21G*, see Ref. 13) and phosphorus ([DURAND]-21G*, see Ref. 13) and with 41G for oxygen ([DURAND]-41G, see Ref. 14) and fluorine ([DURAND]-41G, see Ref. 15). These basis sets are denoted here as (a). We also used an ECP for the lanthanum core (see Ref. 16). No f orbitals are included in the lanthanum basis set since CRYSTAL98 is currently unable to handle functions of this angular momentum. For each apatite studied, the outer sp exponents of the valence part of the basis set have been optimized at the experimental geometry. In order to analyze with greater precision the oxygen charges in the $Ca_2La_8(SiO_4)_6O_2$, calculations for this apatite have been carried out by using both the above basis and an all-electron one (except for La), denoted (b), with the following contractions: 86-511G* for calcium, 65-111G* for silicon and 8-51G for oxygen (see Ref. 16). We use high numerical accuracy parameters: values of 7, 7, 7, 8, and 15 have been chosen for the parameters controlling the direct space summations for the Coulomb and exchange series. A shrinking factor of 4 has been used for the sampling of the Brillouin zone, corresponding to a regular mesh of 12**k** points in reciprocal space. Optimization of the structures has been done by using the conjugate gradient method within the restricted Hartree-Fock (RHF) formalism. Mulliken analysis and bond

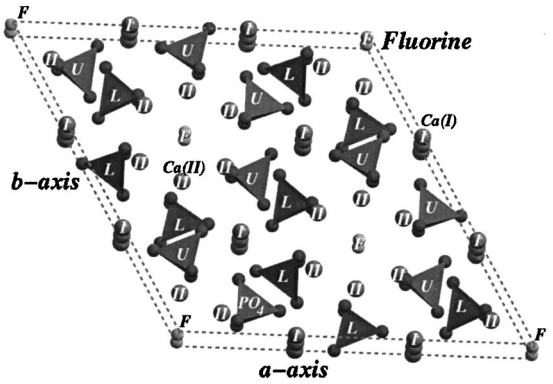

FIG. 1. Supercell composed of four unit cells of $Ca_{10}(PO_4)_6F_2$ viewed towards the ab plane. Calcium atoms are marked with I or II to denote sites I and II, respectively. One phosphate tetrahedron is represented at the bottom of the figure. U and L on phosphate tetrahedra denote upper and lower tetrahedra.

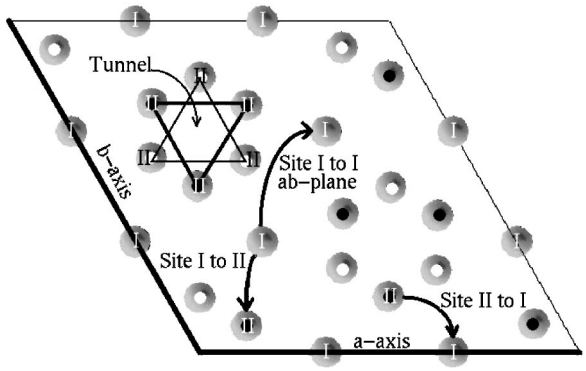

FIG. 2. Cesium migration path (indicated by arrows) from site I to the vacancy at site II, from II to I and from I to I. The conventional unit cell is shown projected on to the ab plane; atoms at site II marked by black or white spots lie in planes with z fractionnal coordinates differing by 0.25. Oxygen, fluorine, silicon, and phosphorus are not represented in this view.

population calculations are used for the optimization of the interionic potentials applied for the investigation of Cs preferential site incorporation and lattice migration in the above apatite structures.

In our previous study,[6] we used interatomic potential techniques as implemented in the program GULP.[8] This approach is capable of determining the location of transition states by applying the rational function optimization (RFO) method. The electrostatic energy is obtained by considering the Coulomb interactions supplemented by short-range potentials. The latter are two-body ionic potentials of the Buckingham type composed of a Born-Mayer repulsive term and an r^{-6} attractive one, as well as three-body harmonic potentials for O-Si-O and O-P-O in order to represent the tetrahedral configuration of oxygen around silicon and phosphorus. Cation-cation interactions are taken to be purely electrostatic. The oxygen ion polarizability is taken into account by using the classical shell model of Dick and Overhauser,[17] following which the interaction between the core and the shell is characterized by a harmonic spring constant.

III. PURE APATITES $Ca_{10}(PO_4)_6F_2$, $Ca_4La_6(SiO_4)_6F_2$ AND $Ca_2La_8(SiO_4)_6O_2$

A. The apatite crystal structure

Apatites are described in the hexagonal symmetry group $P6_3/m$. They are composed of a network of phosphate $[PO_4]^{3-}$ and/or silicate $[SiO_4]^{4-}$ tetrahedra along the c axis (see Fig. 1), linking the cations between them. Cations on the special site $4f$, usually denoted site I, are ninefold oxygen coordinated while cations on site $6h$, denoted site II, are sevenfold coordinated with six oxygen ions and a fluorine. In $Ca_{10}(PO_4)_6F_2$ and $Ca_4La_6(SiO_4)_6F_2$, fluorine ions form an array along the c axis occupying the center of hexagonal tunnels whose section is in the ab-plane and has an approximate diameter of 4 Å. In the case of $Ca_2La_8(SiO_4)_6O_2$ the oxygen ions substitute for fluorines in the tunnels and are denoted O_T. For the migration analysis, it is worth noticing that Ca(I) lies on a threefold axis; it has three nearest neighbors of type Ca(I) in the basal ab plane (see Fig. 2), two other Ca(I) along the c axis, and six nearest neighbors Ca(II). Ca(II) lies on a mirror plane and has four nearest neighbors of Ca(I) and eight Ca(II) (see Fig. 3). Among these last ions, two are in the basal plane creating the possibility of *cyclic* lattice migration in the presence of vacancies (see Fig. 3), while four other Ca(II) ions will produce *diagonal* migration, and finally two nearest neighbors are situated along the c axis.

B. *Ab initio* calculations

The pure apatites $Ca_{10}(PO_4)_6F_2$, $Ca_4La_6(SiO_4)_6F_2$, and $Ca_2La_8(SiO_4)_6O_2$ have been optimized with the CRYSTAL98 code and the results for the lattice volumes, internal parameters, and interatomic distances are presented in Tables I, II, and III, respectively. As expected,[11] due to the fact that the correlation energy is not taken into account, the Hartree-Fock calculations overestimate the volumes of the structures (see Table I) compared to the corresponding experimental ones. Nevertheless, it is worth noticing that the internal parameters obtained for $Ca_{10}(PO_4)_6F_2$ with CRYSTAL98 (quoted in Table II) are very close to the experimental ones, leading to quite satisfactory calculated distances for Ca-O, Ca-F, and P-O (quoted in Table III), whose relative differ-

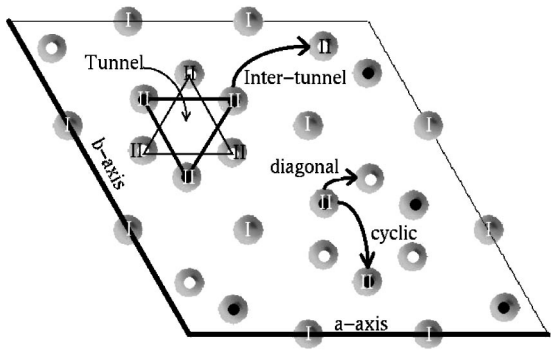

FIG. 3. Cesium migration path from site II to site II. Symbols are the same as in Fig. 2.

TABLE I. Comparison between experimental (Expt.) and calculated lattice parameters and volumes for the three apatites considered within Hartree-Fock (HF) and interatomic based potentials (IP) methods.

	HF	IP	Expt.
$Ca_{10}(PO_4)_6F_2$	Pseudopotential basis sets[a]	O_T shell	
Vol. (Å^3)	551.5 (+5.2%)	522.2 (-0.4%)	524.2 (Ref. 41)
a(Å)	9.5928	9.3688	9.3671
c(Å)	6.9203	6.8995	6.8841
$Ca_4La_6(SiO_4)_6F_2$	Pseudopotential basis sets[a]	O_T shell	
Vol. (Å^3)	612.5 (+6.4%)	579.5 (+0.6%)	575.9 (Ref. 41)
a(Å)	9.8636	9.7702	9.650
c(Å)	7.2696	7.0339	7.141
$Ca_2La_8(SiO_4)_6O_2$	Pseudopotential basis sets[a]	O_T shell	
Vol. (Å^3)	620.2 (+7.5%)	596.3 (+3.4%)	576.8 (Ref. 42)
a (Å)	9.8800	9.8692	9.651
c (Å)	7.3361	7.0688	7.151
$Ca_2La_8(SiO_4)_6O_2$	All-electrons basis sets[b]	O_T core/formal charge	
Vol. (Å^3)	619.3 (+7.4%)	581.2 (+0.8%)	576.8 (Ref. 42)
a(Å)	9.8709	9.7181	9.651
c(Å)	7.3393	7.1055	7.151

[a]La ECP (see Ref. 16), Ca [HAYWSC]-211G*, Si [DURAND]-21G*, and O [DURAND]-41G (see references in text).

[b]La ECP, Ca 86-511G*, Si 65-111G*, and O 8-51G (see Ref. 16).

ences compared to the experimental values are roughly of the order of 10^{-2}. The binding energy (BE), defined as the difference between the total energy of the solid and the sums of the isolated atomic energies, has been calculated for $Ca_{10}(PO_4)_6F_2$, both at the Hartree-Fock (HF) level and with *a posteriori* correction for correlation using the Perdew-Wang functional PW91 (see Refs. 7, 18 and 19) yielding $E^{\mathrm{BE}}_{Ca_{10}(PO_4)_6F_2}(\mathrm{HF})=5.45$ hartree and $E^{\mathrm{BE}}_{Ca_{10}(PO_4)_6F_2}(PW91//\mathrm{HF})=7.68$ hartree, respectively. These values represent 57% and 81%, respectively, of the experimental value $E^{\mathrm{BE}}_{Ca_{10}(PO_4)_6F_2}(\mathrm{expt})=9.54$ Hartree (Ref. 20) in accordance with the typical underestimations obtained when using the present approach.[11] To our knowledge, no experimental data are available for the $Ca_4La_6(SiO_4)_6F_2$ and $Ca_2La_8(SiO_4)_6O_2$ internal parameters, interatomic distances, and BE's. However, based on the results obtained for $Ca_{10}(PO_4)_6F_2$ and also on the fact that the calculated Si-O distances in $Ca_4La_6(SiO_4)_6F_2$ and $Ca_2La_8(SiO_4)_6O_2$ are very close to 1.62 Å as expected (see Ref. 21), we may consider the optimization of the $Ca_4La_6(SiO_4)_6F_2$ and $Ca_2La_8(SiO_4)_6O_2$ structures to be satisfactory on the whole. Furthermore, the calculation of the BE for the last two apatites cannot be carried out since the HF energy for lanthanum as an isolated neutral atom needs to consider the *f* orbitals, which cannot be included in the present work.

The Mulliken analysis of the charges for all the sublattices has been performed at the optimized geometries obtained within the *ab initio* Hartree-Fock method for all the three apatites considered. The results are reported in Table IV. The total charges of calcium and lanthanum ions located either at sites I or II are very close to the formal ones, +2 and +3, respectively, while those of silicon, phosphorus, and oxygen in the tetrahedra are far from their ideal values, +4, +5, and −2, respectively. It is important to notice that the total

TABLE II. Comparisons between experimental internal parameters[41] and calculated values obtained using the Hartree-Fock method for $Ca_{10}(PO_4)_6F_2$ and basis sets outlined in footenote a (see Table I).

$Ca_{10}(PO_4)_6F_2$ site	Ca(I) $4f$	Ca(II) $6h$	P $6h$	O_1 $6h$	O_2 $6h$	O_3 $12i$	F $2a$
$x_{\mathrm{calc.}}$	1/3	0.2443	0.3994	0.3358	0.5857	0.3407	0.0
$x_{\mathrm{expt.}}$	*1/3*	*0.2416*	*0.3981*	*0.3262*	*0.5880*	*0.3416*	*0.0*
$y_{\mathrm{calc.}}$	2/3	−0.0063	0.3709	0.4899	0.4624	0.2607	0.0
$y_{\mathrm{expt.}}$	*2/3*	*0.0071*	*0.3688*	*0.4843*	*0.4668*	*0.2468*	*0.0*
$z_{\mathrm{calc.}}$	0.0045	1/4	1/4	1/4	1/4	0.0714	1/4
$z_{\mathrm{expt.}}$	*0.0011*	*1/4*	*1/4*	*1/4*	*1/4*	*0.0704*	*1/4*

TABLE III. Calculated cation-anion distances (in Å) for the three apatites considered, obtained using the Hartree-Fock method [with basis sets outlined in footnote a (Table I)]. Values in parenthesis correspond to the experimental data for $Ca_{10}(PO_4)_6F_2$, the numbers in brackets indicate the number of distances, while O_T implies oxygen in the tunnel.

	$Ca_{10}(PO_4)_6F_2$		$Ca_4La_6(SiO_4)_6F_2$		$Ca_2La_8(SiO_4)_6O_2$	
Ca_I-O	2.409 [3] (2.397)	2.490 [3] (2.453)	2.495 [3]	2.525 [3]	2.532 [3]	2.598 [3]
	2.891 [3] (2.801)		3.067 [3]		2.922 [3]	
La_I-O					2.516 [3]	2.576 [3]
						2.921 [3]
Ca_{II}-O	2.363 [2] (2.384)	2.442 [1] (2.384)				
	2.564 [2] (3.398)	2.829 [1] (2.814)				
Ca_{II}-F	2.374 (2.231)					
La_{II}-O			2.429 [2]	2.499 [1]	2.532 [2]	2.498 [1]
			2.611 [2]	3.365 [1]	2.661 [2]	2.820 [1]
La_{II}-F,O_T			2.516		2.399	
P-O,Si-O	1.539 [2] (1.534)	1.540 [1] (1.541)	1.619 [2]	1.606 [1]	1.632 [2]	1.604 [1]
	1.548 [1] (1.534)		1.618 [1]		1.647 [1]	

charge of fluorines as well as those of oxygen O_T ions along the *c* axis, in the tunnel, (see Table IV) are very close to the formal values, -1 and -2, respectively. In fact, both basis sets give quite close results for the O_T charges in $Ca_2La_8(SiO_4)_6O_2$ (see Table IV). Hence, the charge on O_T contrasts with the values obtained for the oxygens located in other sites in the bulk belonging to silicate and phosphate tetrahedra, for which the calculated charges are between -1.3 and $-1.6|e|$. The calculated bond populations along Ca-O bonds are very close to zero, witnessing a strong ionic nature in agreement with Ref. 22. A small part of covalence (in agreement with Ref. 23) is noted for the Ca-F and La-F bonds though overall the interaction can be characterized as ionic. Conversely, the bond populations are considerably higher for the Si-O and P-O bonds in the tetrahedra, varying between $0.2|e|$ and $0.4|e|$. Consequently, the Si-O and P-O bonds appear to have mostly a covalent character, as expected.[21,24]

C. Interatomic potential (IP) modeling

Due to the hexagonal symmetry along the *c* axis, and specifically the presence of inversion symmetry, the interactions between anions F^{1-} or O_T^{2-} in the tunnels and cations Ca^{2+} or La^{3+} at sites II may be described in an appropriate way by using rigid cores with formal charges and Buckingham potentials. Consequently, for the modeling of $Ca_{10}(PO_4)_6F_2$ and $Ca_4La_6(SiO_4)_6F_2$ we use the force field given in Table V (see Ref. 6) with the constraints that fluorines, calcium, and lanthanum ions are considered as rigid cores with formal charges. For the La-O interaction we use the ionic potential established by Lewis and Catlow.[25] For the phosphate and silicate tetrahedra we assessed that there was no value in introducing covalent potentials since the previously parametrized shell model representation gives quite good results for their description.[6] The corresponding optimized structures are in good agreement with the experimental values as shown in Table I. Optimization of the

TABLE IV. Mulliken charges for the atoms in the three apatites calculated within the HF method at the optimized geometries. Both basis sets, (a) and (b), give equivalent results for calcium ions as well as for oxygen ion O_T in the tunnel.

Charges $\|e\|$	$Ca_{10}(PO_4)_6F_2$	$Ca_4La_6(SiO_4)_6F_2$	$Ca_2\ La_8(SiO_4)_6O_2$
Site I	Ca: $+1.98$[a]	Ca: $+1.99$[a]	Ca: $+1.98$ [a]/La: $+3.00$[a]
			Ca: $+1.94$ [b]/La: $+3.00$[b]
Site II	Ca: $+1.98$[a]	La: $+3.00$[a]	La: $+3.00$[a]
			La: $+3.00$[b]
Tetrahedra	P: $+1.35$[a]	Si: $+1.90$[a]	Si: $+1.75$[a]
			Si: $+2.00$[b]
Oxygen	-1.06 [a]/-1.12[a]	-1.42 [a]/-1.51[a]	-1.29 [a]/-1.55[a]
			-1.36 [b]/-1.50[b]
Tunnel	F: -0.99[a]	F: -0.99[a]	O_T: -1.97[a]
			O_T: -1.98[b]

[a]La ECP (see Ref. 16), Ca [HAYWSC]-211G*, Si [DURAND]-21G*, and O [DURAND]-41G (see references in text).

[b]La ECP, Ca 86-511G*, Si 65-111G*, and O 8-51G (see Ref. 16).

TABLE V. Potentials parameters for the three apatites considered. Charges are $O_{core}=+0.86$, $O_{shel}=-2.86$ with $k_{O\ core\text{-}O\ shel}=98.67$ eV Å^{-2}, $O_{T,core}=-2.0$, $Ca_{core}=+2.0$, $La_{core}=+3.0$, $Si_{core}=+4.0$, $P_{core}=+5.0$, $F_{core}=-1.0$, $Cs_{core}=+1.0$. The three-body harmonic potentials are $k_{O\ shel\text{-}P\ core\text{-}O\ shel}=2.840$ eV rad^{-2} with $\theta_0=109.5$ deg. and $k_{O\ shel\text{-}Si\ core\text{-}O\ shel}=16.675$ eV rad^{-2} with $\theta_0=109.5°$.

	O-O	La-O	La-O_T	Ca-O	P-O	Si-O	Cs-O
A (eV)	22764.3	1439.7	1439.7	1288.2	836.5	1076.7	15085.5
ρ (Å)	0.1490	0.3661	0.3363	0.3316	0.3513	0.3147	0.2549
C (eV Å^6)	32.58	0.00	0.00	0.00	0.00	0.00	0.00
	F-F	F-O	La-F	Ca-F	P-F	Si-F	Cs-F
A (eV)	1128.0	198.3	8179.3	2030.6	697.4	242.8	3124.9
ρ (Å)	0.2753	0.1110	0.2583	0.2711	0.2389	0.3450	0.3000
C (eV Å^6)	0.00	0.00	0.00	0.00	0.00	0.00	0.00

$Ca_2La_8(SiO_4)_6O_2$ structure employing a shell model for the oxygens in the tunnels identical to that used in the phosphate or silicate tetrahedra overestimates the lattice volume by roughly 3%. The introduction of a rigid core for oxygen in the tunnel O_T and a slight adjustment of the Buckingham ρ parameter to 0.3363 Å significantly improves the calculated volume (Table I) whose relative difference from the experimental value becomes less than 1%. This model is in qualitative agreement with the *ab initio* calculations for F and O_T anions, as well as Ca and La cations, while it preserves the already satisfactory shell model representation for phosphate and silicate groups.[6]

IV. CESIUM INCORPORATION AND LATTICE MIGRATION IN $Ca_{10}(PO_4)_6F_2$, $Ca_4La_6(SiO_4)_6F_2$, AND $Ca_2La_8(SiO_4)_6O_2$

A. Cesium incorporation

In order to keep the systems charge neutral, the combination of a cesium and a lanthanum ion (Cs^+,La^{3+}) can be substituted for two calcium ions (2 Ca^{+2}) in $Ca_{10}(PO_4)_6F_2$, $Ca_4La_6(SiO_4)_6F_2$, and $Ca_2La_8(SiO_4)_6O_2$. The main difficulty comes from the fact that multiple configurations are possible for this substitution. Experimental evidences[22,26–30] have shown that 75% of sites II are preferentially occupied by rare earth elements (R) rather than calcium. Generally, the range of the ratio (number of R ions at site II)/(number of R at site I) lies between 1.76 and 3.00.[31] Furthermore, a previous theoretical study[6] on the apatite $Ca_9Nd(SiO_4)(PO_4)_5F_2$ has also confirmed this tendency by showing the free energy of the system to be considerably lower when Nd ions are substituted at site II rather than at site I.

The first step consists of determining the most probable site for each cation substitution in the three apatites of interest in this paper. Applying a method equivalent to Ref. 6 we have calculated the Helmholtz free energies $A_T=U_{\text{lattice}}-TS_{\text{vib}}$, at $T=300$ K, for various configurations of the three apatites and compared to that of a reference configuration in which Cs occupies site I while all the site II are occupied by Ca ions in $Ca_{10}(PO_4)_6F_2$ and La ions in $Ca_4La_6(SiO_4)_6F_2$ /$Ca_2La_8(SiO_4)_6O_2$. U_{lattice} corresponds to the internal energy and S_{vib} is the vibrational entropy for the supercells of the corresponding configurations, calculated at the Γ point of the Brillouin zone by using the phonon spectra. The results are quoted in Table VI. The first two lines (Table VI) indicate that Cs prefers to lie at site I rather than site II, whatever the compound considered. Conversely, the relative Helmholtz free energies for Ca and La at sites I and II and vice versa show a preference for La to occupy site II. These results show a good correlation with the experimental evidence[22,27–30] and previous theoretical considerations.[6]

B. Cesium lattice migration

For the Cs lattice migration study in $Ca_{10}(PO_4)_6F_2$, $Ca_4La_6(SiO_4)_6F_2$, and $Ca_2La_8(SiO_4)_6O_2$, three pairs of (Cs^+, La^{3+}) have been substituted for three calcium pairs (2 Ca^{+2}) in a supercell comprising eight conventional unit cells, thus yielding the following Cs-doped compositions: $Ca_{74}Cs_3La_3(PO_4)_{48}F_{16}$, $Ca_{26}Cs_3La_{51}(SiO_4)_{48}F_{16}$ and $Ca_{10}La_{67}Cs_3(SiO_4)_{48}O_{16}$. These correspond to roughly 3 wt % of Cs concentration. In order to respect the site preferences of cesium and lanthanum in these structures, two Cs^+ ions have been substituted at site I and 70% of La^{3+} ions at

TABLE VI. Helmholtz free energy differences at 300 K between different configurations corresponding to the incorporation of cesium or lanthanum at calcium site I or site II. The lowest-energy configuration, with Cs at site I and La at site II, is considered as the energy reference and set to zero.

Relative Helmholtz free energies (kJ mol^{-1})	$Ca_{10}(PO_4)_6F_2$	$Ca_4La_6(SiO_4)_6F_2$	$Ca_2La_8(SiO_4)_6O_2$
$A_{300\ K}$[Cs(I)/Ca(II);La(II)] − $A_{300\ K}$[Cs(II)/Ca(I)]	+28.0	+58.6	+16.4
$A_{300\ K}$[Cs(I)/Ca(II);La(II)] − $A_{300\ K}$[Cs(II)/La(I)]	+71.4	+197.8	+26.1
$A_{300\ K}$[Ca(I)/La(II)] − $A_{300\ K}$[Ca(II)/La(I)]	+40.5	+72.4	+75.3

TABLE VII. Activation energies (in eV) for cesium migration initially situated at site I Cs(I) or at site II Cs(II) to adjacent vacancies V''_{Ca}(I) and V'''_{La}(I) calculated within the Mott-Littleton approach (Ref. 33) for the three apatites considered. The migration paths are represented in Figs. 2 and 3, except for the migration along the *c* axis.

V''_{Ca}(I)	$Ca_{74}Cs_3La_3(PO_4)_{48}F_{16}$	$Ca_{26}Cs_3La_{51}(SiO_4)_{48}F_{16}$	$Ca_{10}La_{67}Cs_3(SiO_4)_{48}O_{16}$
Cs(I) $\rightarrow ab$	0.81	1.73	2.86
Cs(I) $\rightarrow c$	0.99	1.92	2.85
Cs(II) $\rightarrow$ site I	0.54	0.60	1.30
V'''_{La}(I)		$Ca_{26}Cs_3La_{51}(SiO_4)_{48}F_{16}$	$Ca_{10}La_{67}Cs_3(SiO_4)_{48}O_{16}$
Cs(I) $\rightarrow ab$		1.50	2.82
Cs(I) $\rightarrow c$		1.89	2.83
Cs(II) $\rightarrow$ site I		1.23	1.85

site II. The resulting ratio (number of *R* ions at site II)/(number of *R* ions at site I) is close to two, in agreement with Ref. 31.

Cesium migration towards adjacent vacancies is investigated by using interatomic potentials. The saddle point search is carried out by the rational function optimization method (RFO).[32] According to this method, the Cs ion is displaced from its equilibrium position towards the adjacent vacancy through calculation at each position the eigenvalues of the Hessian, the energy second derivative matrix. A first-order transition state corresponds to a single imaginary eigenvalue of the Hessian. Calculations are done within the Mott-Littleton approximation,[33] following which the region surrounding the defects, considered to be the displaced cesium ion between the two vacancies, is divided into three concentric spherical regions. In the first one all the interactions are considered explicitly and ions are allowed to relax fully. In the second one, only harmonic relaxations are considered, and in the third one, ions respond to the defect net charge as a series of polarizable sublattices. For our calculations, the first sphere has a radius of 9 Å and contains about 240 atoms, while the second sphere has a radius of 20 Å containing about 2400 ions.

We have formally distinguished two principal migration possibilities for Cs: towards cation (Ca or La) vacancies located at sites I and at site II. For both situations, results are quoted in Tables VII and VIII with the corresponding paths illustrated in Figs. 2 and 3, respectively. Evidently, Ca or La vacancies do not have an equal importance for the Cs migration in all the above compositions. Since in $Ca_{74}Cs_3La_3(PO_4)_{48}F_{16}$ more than 92% of cations are calcium (lying either at site I or II), cesium migration towards lanthanum vacancies in this compound has not been considered. Conversely, for $Ca_{26}Cs_3La_{51}(SiO_4)_{48}F_{16}$ and $Ca_{10}La_{67}Cs_3(SiO_4)_{48}O_{16}$, both calcium and lanthanum vacancies play an important role in cesium lattice migration as shown in Tables VII and VIII.

Cesium located at site I, denoted Cs(I), may migrate to Ca or La vacancies at site I, V''_{Ca}(I) or V'''_{La}(I), either in the *ab* plane or along the *c* axis (see Fig. 2). In both directions, and

TABLE VIII. Activation energies (in eV) for migration of cesium (situated at site II or site I) upon adjacent vacancies V''_{Ca}(II) and V'''_{La}(II), calculated within the Mott-Littleton approach (Ref. 33) for the three apatites considered. The migration paths are represented in Figs. 2 and 3, except for migration along the *c* axis. Labels (La) and (Ca) for *cyclic* diffusion to site II for $Ca_{10}(PO_4)_6F_2$ indicate cesium migration near La and Ca, respectively.

V''_{Ca}(II)	$Ca_{74}Cs_3La_3(PO_4)_{48}F_{16}$	$Ca_{26}Cs_3La_{51}(SiO_4)_{48}F_{16}$	$Ca_{10}La_{67}Cs_3(SiO_4)_{48}O_{16}$
Cs(I) $\rightarrow$ site II	0.94	1.10	2.25
Cs(II) $\rightarrow$ inter-tunnel	0.51,0.85	0.67	2.57
Cs(II) $\rightarrow diagonal$	1.00	0.35	2.00
Cs(II) $\rightarrow c$	0.57	1.34	-
Cs(II) $\rightarrow cyclic$	4.15 (La),1.15 (Ca)	1.83	-
V'''_{La}(II)		$Ca_{26}Cs_3La_{51}(SiO_4)_{48}F_{16}$	$Ca_{10}La_{67}Cs_3(SiO_4)_{48}O_{16}$
Cs(I) $\rightarrow$ site II		0.78	1.08
Cs(II) $\rightarrow$ inter-tunnel		1.18	2.73
Cs(II) $\rightarrow diagonal$		1.67	1.60
Cs(II) $\rightarrow c$		1.00	3.29
Cs(II) $\rightarrow cyclic$		0.56	0.63,1.22

whatever the cation vacancy considered, the intrasite (I↔I) activation energies are close for the same apatite: around 0.8–1.0 eV in $Ca_{10}(PO_4)_6F_2$ (see Table VII), 1.5–1.9 eV for $Ca_4La_6(SiO_4)_6F_2$, and 2.8 eV for $Ca_2La_8(SiO_4)_6O_2$. For Cs(I) migration towards vacancies at sites II, V''_{Ca}(II) or V'''_{La}(II), the corresponding activation energies are of the same order for $Ca_{10}(PO_4)_6F_2$, that is, 0.94 eV, but slightly lower when compared to intrasite (I↔I) diffusion, for $Ca_4La_6(SiO_4)_6F_2$, 0.78–1.1 eV, and $Ca_2La_8(SiO_4)_6O_2$, 1.08–2.25 eV (see Table VIII). For the intrasite transition in the *ab* plane, it is worth noticing the constant increase of the activation energies, from $Ca_{10}(PO_4)_6F_2$ to $Ca_4La_6(SiO_4)_6F_2$ and then to $Ca_2La_8(SiO_4)_6O_2$, mainly due to the influence of La and silicate groups when substituted for Ca and phosphates.

There are at least four paths for Cs(II) migration from site II to vacancies lying at site II (intrasite diffusion: II ↔II), intertunnel displacement as quoted in Table VIII and pictured in Fig. 3, along the *c* axis (intratunnel) by shifting the *z* fractional coordinate by 0.5 (denoted *c* in Table VIII), *diagonal* displacement (denoted *diagonal*) corresponding to jumping from site II to site II by shifting the *z* fractional coordinate by 0.25 and rotating by 60°, and finally, *cyclic* displacement, following which cesium may migrate from site II to site II vacancies with equal *z* fractional coordinate (see Fig. 3). The calculated activation energies corresponding to each path are presented in Table VIII. Once more the highest activation energies are obtained in $Ca_2La_8(SiO_4)_6O_2$.

Comparison of the intertunnel activation energies for cesium diffusion (Table VIII), shows that they are almost equivalent in $Ca_{10}(PO_4)_6F_2$ and $Ca_4La_6(SiO_4)_6F_2$, but considerably higher in the case of $Ca_2La_8(SiO_4)_6O_2$, demonstrating the strong influence of the oxygen ions in the tunnels with respect to the fluorines ones. However, it appears difficult to distinguish the influence of various sublattices in the case of *diagonal* and *c* axis diffusion since the contribution of the first and second neighbor interactions on the migration path is due to the cations at sites II, around the tunnel (see Fig. 1), to the nature of the anion along the *c*-axis in the tunnel and finally to the type of tetrahedra, phosphate or silicate, distributed around the tunnel.

The magnitude of the activation energies for intersite (I ↔II) diffusion is roughly lower than that for intrasite ones, for the three apatites considered. Intersite migration appears then as the most probable mechanism for the cesium lattice diffusion in these apatites. In order to simplify the behavior of cesium migration in $Ca_{10}(PO_4)_6F_2$, $Ca_4La_6(SiO_4)_6F_2$, and $Ca_2La_8(SiO_4)_6O_2$, a scheme has been given in Fig. 4, quoting the lowest activation energies for each migration path. We also observe an increase of the activation energies by 0.8 eV for intrasite diffusion site I and by 0.5 eV for intrasite diffusion site II, with the following order $Ca_{10}(PO_4)_6F_2$, $Ca_4La_6(SiO_4)_6F_2$ and $Ca_2La_8(SiO_4)_6O_2$. Moreover, we can add that *cyclic* cesium diffusion in $Ca_{10}(PO_4)_6F_2$ near La has a higher activation energy than that near Ca as shown by the last line in Table VIII, demonstrating the clear influence of the La ions in this kind of migration path.

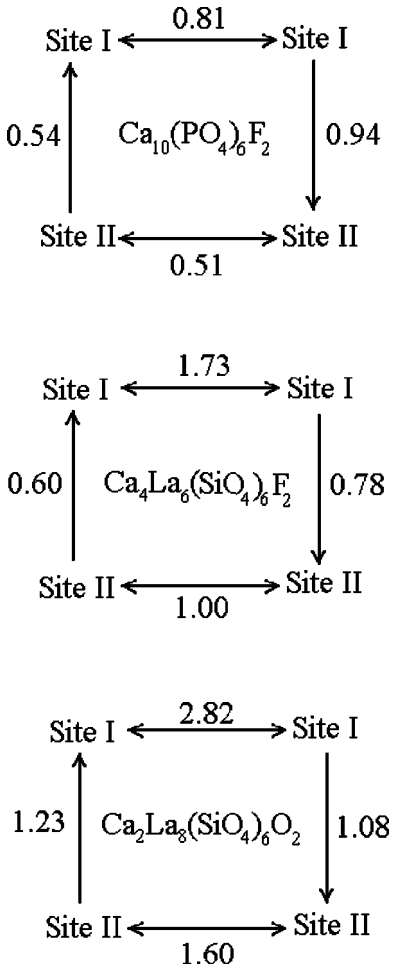

FIG. 4. Simplified scheme for the lowest computed activation energies for Cs^+ lattice migration towards adjacent vacancies (V''_{Ca} or V'''_{La}) located at sites I and II for the three apatites considered. Activation energies are quoted in eV.

Within the Arrhenius approximation, the temperature dependence of the diffusion is characterized not only by the lattice migration activation energies (E_a) but also by a prefactor coefficient D_0 following the well known relation[34] $D = D_0\, e^{-E_a/(k_B T)}$ (k_B being Boltzmann's constant). Here, D_0 mainly depends on the cesium-vacancy distances ($d_{\text{Cs-V}_{\text{Ca,La}}}$), the cesium vibration frequencies (ν_{Cs}), and the activation entropy for migration ΔS_a,[35] according to $D_0 \propto d^2_{\text{Cs-V}_{\text{Ca,La}}}\, \nu_{Cs} e^{\Delta S_a/(k_B T)}$. Cesium ions vibrational frequencies ν_{Cs} at their equilibrium positions, involved in the prefactor D_0, have been estimated by considering the zero-point vibration energies along the three directions for Cs when located at site I, as well as at site II. Results, quoted Table IX for the three apatites, show that no clear tendency can be extracted from the values obtained since they are all very close to each other. Furthermore, for the apatites considered cesium-vacancy distances are very close: for example the $d_{\text{Cs-V}_{\text{Ca,La I}}}$ along the *c* axis are roughly 3.4, 3.5, and 3.6 Å, for $Ca_{10}(PO_4)_6F_2$, $Ca_4La_6(SiO_4)_6F_2$, and $Ca_2La_8(SiO_4)_6O_2$, respectively. Last, the activation entropies for migration ΔS_a are usually $< 5k_B$,[35–37] which at 300 K roughly corresponds

TABLE IX. Zero-point energies corresponding to the vibrational frequencies of cesium along *x*, *y*, and *z* coordinates, in the two sites for the three apatites considered.

E_{Cs} (cm^{-1})	$Ca_{74}Cs_3La_3(PO_4)_{48}F_{16}$	$Ca_{26}Cs_3La_{51}(SiO_4)_{48}F_{16}$	$Ca_{10}La_{67}Cs_3(SiO_4)_{48}O_{16}$
Site I	116.8,118.7,146.4	100.2,111.5,147.5	106.4,108.7,146.5
Site II	104.2,134.6,140.3	108.7,111.1,151.0	106.9,107.9,148.2
Site II	100.5,108.8,128.3	92.4,109.3,122.6	85.8,113.0,127.7

to 0.1 eV, having thus not significant influence to the migration probability when compared to the calculated activation energies. In fact, in the transition state theory this quantity is generally set to zero.[38,39] Consequently, we may consider that the activation energies for the various lattice migration mechanisms are quite sufficient for discriminating the most efficient apatite for cesium immobilization.

Finally, the general picture obtained is that $Ca_2La_8(SiO_4)_6O_2$ has a higher capacity for confining cesium, from a diffusional point of view, compared to $Ca_{10}(PO_4)_6F_2$ and to $Ca_4La_6(SiO_4)_6F_2$. Indeed, in most of the migration mechanisms investigated above, the corresponding activation energies characterizing cesium migration in $Ca_2La_8(SiO_4)_6O_2$ are considerably higher than those in the two other apatites (see Fig. 4). Moreover, experimental data on oxyapatites synthesis[40] show that, for increasing concentration of La ions, the oxygen vacancy concentration in the tunnel decreases. This result can be qualitatively transposed to $Ca_2La_8(SiO_4)_6O_2$, where a very low oxygen vacancy concentration would be expected in the tunnels and consequently a quite efficient Cs immobilization in this structure.

V. CONCLUSION

Three apatites $Ca_{10}(PO_4)_6F_2$, $Ca_4La_6(SiO_4)_6F_2$, and $Ca_2La_8(SiO_4)_6O_2$ have been studied theoretically in order to give insight as to their ability to incorporate and immobilize cesium in their structure. Based on periodic *ab initio* Hartree-Fock calculations for the characterization of the anion charges in the apatite tunnels, as well as for the nature of the bonds with the cations situated at site II, we have established a force field that satisfactorily describes the three apatites. The interionic potentials used are based on a rigid ion model for fluorine and oxygen in the tunnels along the *c* axis and on a shell model for the silicate and phosphate tetrahedra. Using the resulting interatomic potentials, we have calculated the Helmholtz free energies at 300 K of various relaxed structures, with configurations of Cs and La at sites I and II and vice versa. Comparison of the results obtained provides evidence that cesium ions substitute with a slight preference for site I over site II, whatever the apatite considered. Conversely, lanthanum ions have a net preference for site II. These results are in agreement with previous experimental works and theoretical considerations.

A detailed study has been carried out on a number of possible mechanisms for the cesium lattice migration in doped $Ca_{10}(PO_4)_6F_2$, $Ca_4La_6(SiO_4)_6F_2$ and $Ca_2La_8(SiO_4)_6O_2$. For that purpose, we have considered the compositions $Ca_{74}Cs_3La_3(PO_4)_{48}F_{16}$, $Ca_{26}Cs_3La_{51}(SiO_4)_{48}F_{16}$, and $Ca_{10}La_{67}Cs_3(SiO_4)_{48}O_{16}$, with periodic boundary conditions, corresponding to 3 wt % of Cs concentration. In these structures, we have respected the site preferences for Cs and La by considering 75% of lanthanum ions occupying sites II and two cesium ions among the three located at sites I. The calculation of the activation energies characterizing the corresponding migration paths considered towards adjacent cation vacancies indicates that cesium lattice diffusion is mostly controlled by intersite mechanisms (I↔II). The calculated vibrational zero-point energies at equilibrium in all the three apatites are of the same magnitude as well as the cesium-vacancy distances and consequently they have no influence on any preferential crystallographic direction for migration. Finally, comparison of the activation energies obtained for all the possible migration mechanisms clearly demonstrates that the lanthanum oxyapatite $Ca_2La_8(SiO_4)_6O_2$ exhibits the higher immobilization capacity for cesium, compared to fluoroapatite $Ca_{10}(PO_4)_6F_2$ and lanthanum-fluorobritholite $Ca_4La_6(SiO_4)_6F_2$.

[1] R. Bros, J. Carpena, V. Sere, and A. Beltritti, Radiochim. Acta **74**, 277 (1996).
[2] J. Carpena and J. L. Lacout, Licence graduate (1993).
[3] R. C. Ewing, W. J. Weber, and W. Lutze, *Disposal of Weapons Plutonium* (Kluwer Academic, The Netherlands, 1996).
[4] L. Boyer, J. Carpena, and J. L. Lacout, Licence graduate (1998).
[5] N. Sénamaud, Ph.D. thesis, Université de Limoges, France (1999).
[6] C. Meis, J.D. Gale, L. Boyer, J. Carpena, and D. Gosset, J. Phys. Chem. A **104**, 5380 (2000).
[7] V.R. Saunders, R. Dovesi, C. Roetti, M. Causà, N.M. Harrisson, R. Orlando, and C.M. Zicovich-Wilson, CRYSTAL98 User's Manual (University of Torino, Torino, 1998).
[8] J.D. Gale, J. Chem. Soc., Faraday Trans. **93**, 629 (1997).
[9] E.V. Stefanovich, A.L. Shluger, and C.R.A. Catlow, Phys. Rev. B **49**, 11 560 (1994).
[10] S. Tsuneyuki, M. Tsukada, H. Aoki, and Y. Matsui, Phys. Rev. Lett. **61**, 869 (1988).
[11] R. Dovesi, C. Roetti, C. Freyra-Fava, E. Aprà, V.R. Saunders, and N.M. Harrisson, Philos. Trans. R. Soc. London, Ser. A **341**, 203 (1992).

[12] M. P. Habas, R. Dovesi, and A. Lichanot, J. Phys.: Condens. Matter **10**, 6897 (1998).
[13] M. Causà, R. Dovesi, and C. Roetti, Phys. Rev. B **43**, 11 937 (1991).
[14] E. Aprà, Ph.D. thesis, University of Torino (1992).
[15] M. Nizam, Y. Bouteiller, B. Silvi, C. Pisani, M. Causà, and R. Dovesi, J. Phys. C **21**, 5351 (1988).
[16] S. Bordiga, web site http://www.ch.unito.it/ifm/teorica/BasisSets.
[17] B. Dick and A. Overhauser, Phys. Rev. **112**, 90 (1958).
[18] J. P. Perdew, *Electronic Structure of Solids 91* (Springer, Berlin, 1991).
[19] J. P. Perdew, J.A. Chevary, S.H. Vosko, Koblar A. Jackson, M.R. Pederson, D.J. Singh, and C. Fiolhais, Phys. Rev. B **46**, 6671 (1992).
[20] D. D. Wagman, Natl. Stand. Ref. Data Ser. (U.S. Natl. Bur. Stand.) **11**, (2) (1982).
[21] R. Nada, C.R.A. Catlow, R. Dovesi, and C. Pisani, Phys. Chem. Miner. **17**, 353 (1990).
[22] L. Boyer, B. Piriou, J. Carpena, and J.L. Lacout, J. Alloys Compd. **311**, 143 (2000).
[23] V. Louis-Achille, Ph. D. thesis, Université Paris XI (1999).
[24] R. Dovesi, C. Pisani, C. Roetti, and B. Silvi, J. Chem. Phys. **86**, 6967 (1987).
[25] G. Lewis and C.R.A. Catlow, J. Phys. C **18**, 1149 (1985).
[26] P. Martin, G. Carlot, A. Chevarier, C. Den-Auwer, and G. Panczer, J. Nucl. Mater. **275**, 268 (1999).
[27] G.J. Blasse, J. Solid State Chem. **14**, 181 (1975).
[28] J. Lin and Q. Su, J. Alloys Compd. **210**, 159 (1994).
[29] J. Lin and Q. Su, Mater. Chem. Phys. **38**, 98 (1994).
[30] L. Boyer, J.M. Savariault, J. Carpena, and J.L. Lacout, Acta Crystallogr., Sect. C: Cryst. Struct. Commun. **54**, 1057 (1998).
[31] M. E. Fleet and Y. Pan, J. Solid State Chem. **112**, 78 (1994).
[32] A. Banarjee, N. Adams, J. Simons, and R. Shepard, J. Phys. Chem. **89**, 52 (1985).
[33] N. Mott and M. Littleton, Trans. Faraday Soc. **34**, 485 (1938).
[34] R. M. Barrer, *Diffusion In and Through Solids* (Cambridge University Press, Cambridge, 1951).
[35] T. W. Dobson, J. F. Wager, and J. A. Van Vechten, Phys. Rev. B **40**, 2962 (1989).
[36] A. Seeger and K. P. Chilk, Phys. Status Solidi **38**, 3148 (1967).
[37] F. K. Kröger, *The Chemistry of Imperfect Crystals* (North-Holland, Amsterdam, 1974).
[38] A. Satta, F. Willaime, and S. de Gironcoli, Phys. Rev. B **57**, 11 184 (1998).
[39] W. Frank, U. Breier, C. Elsässer, and M. Fähnle, Phys. Rev. Lett. **77**, 518 (1996).
[40] J. Lacout, M. Mikou, and G. Gonel, J. Solid State Chem. **86**, 323 (1990).
[41] L. Boyer, J. Carpena, and J. L. Lacout, Solid State Ionics **95**, 121 (1997).
[42] W. J. Weber and L. M. Wang, Nucl. Instrum. Methods Phys. Res. B **91**, 63 (1994).